TU Delft

Delft University of Technology

Hardware-in-the-Loop experiments in model ice for analysis of ice-induced vibrations of offshore structures

Hammer, T. C.; Hendrikse, H.

DOI
10.1038/s41598-024-68955-x

Publication date
2024

Document Version
Final published version

Published in
Scientific Reports

Citation (APA)
Hammer, T. C., & Hendrikse, H. (2024). Hardware-in-the-Loop experiments in model ice for analysis of ice-induced vibrations of offshore structures. *Scientific Reports*, *14*(1), Article 18327. https://doi.org/10.1038/s41598-024-68955-x

Important note
To cite this publication, please use the final published version (if applicable).
Please check the document version above.

Copyright
Other than for strictly personal use, it is not permitted to download, forward or distribute the text or part of it, without the consent of the author(s) and/or copyright holder(s), unless the work is under an open content license such as Creative Commons.

Takedown policy
Please contact us and provide details if you believe this document breaches copyrights.
We will remove access to the work immediately and investigate your claim.

This work is downloaded from Delft University of Technology.
For technical reasons the number of authors shown on this cover page is limited to a maximum of 10.

scientific reports

Check for updates

OPEN

Hardware-in-the-Loop experiments in model ice for analysis of ice-induced vibrations of offshore structures

T. C. Hammer✉ & H. Hendrikse

The study investigated the use of a Hardware-in-the-Loop (HiL) technique applied in model ice experiments to enable the analysis of offshore structures with low natural frequencies under dynamic ice loading. Traditional approaches were limited by facility capacities and ineffective downscaling of the geometry of the offshore structures. The goal of the present study was to overcome these challenges and to enhance the understanding and explore the applicability of a hybrid testing technique in model ice experiments. To achieve the objective, 204 Hardware-in-the-Loop simulations in model Ice (HiLI) were analyzed. Results showed robust behavior and good performance of the HiLI due to minimal variation in measured delay, normalized root mean square error, and peak tracking error and low magnitudes of such parameters despite alterations in factors such as the choice of the numerical structural model, physical prototype, measurement system, and ice type. Notably, the performance of the HiLI was affected when testing with warm model ice or scaling for harsh ice conditions, attributed to a reduced signal-to-noise ratio and instability of the system, respectively. Experimental identification of the critical delay, along with the application of an analytical stability criterion, revealed that the instability observed, was likely induced by reducing the structural stiffness of the numerical structural model to fulfil the scaling requirements when testing for harsh ice conditions. Additionally, the study showed improved HiLI performance when the physical prototype was in contact with the model ice. This observation was further analyzed and is assumed to be caused by the coupling between the ice and physical prototype, causing a coupled and thus increased eigenfrequency of the physical prototype-ice system.

Keywords Offshore wind turbine, Ice-induced vibrations, Ice-structure interaction, Dynamic ice load, Hybrid testing methods

Offshore structures interacting with level sea ice crushing against the vertical interface of the structure can experience highly non-linear ice-induced vibrations[1]. The analysis of these vibrations is challenging, stemming from the non-existence or being proprietary of comprehensive full-scale data, inadequacies in scaling laws, or restricted capabilities of test facilities for large-scaled experiments. In the past, test setups developed for experimental analysis of ice-induced vibrations consisted of clamping mechanisms, different spring configurations, and modular mass blocks to adjust the physical structural stiffness and mass of the test setup[2–4]. However, these setups reached their limits when it came to investigating offshore structures such as offshore wind turbines, as setups could not achieve the required lowest natural frequencies due to the load and size capacities of ice tank or basin test facilities.

Modern experiments more regularly consider the application of hybrid testing techniques for analysis of rate-dependent loading scenarios of offshore structures. Those techniques minimize the components of a scaled physical structural model. This approach allows for the translation of intricate physical structural elements into the numerical domain, with only those parts directly affected by the environmental hazard being physically represented. In the fields of mechanical and aerospace engineering, particularly in applications like flight simulator development, hybrid testing techniques are often known as HiL simulations[5]. When the concept was transferred to the field of civil engineering, the term pseudo-dynamic testing was introduced[6,7]. The initial form of hybrid testing involved a clear separation of two phases, one dedicated to the application of loads and

Department of Hydraulic Engineering, Faculty of Civil Engineering and Geosciences, Delft University of Technology, Stevinweg 1, 2628 CN Delft, The Netherlands. ✉email: t.c.hammer@tudelft.nl

the other to the calculation of the structural response. This division of phases characterized the method as a quasi-static testing approach. To circumvent the recuperation of reversible processes during the calculation phase, a continuous pseudo-hybrid testing method was introduced[8], meaning that the physical test setup was accompanied by actuators that prevented motion discontinuity. Subsequently, fast continuous pseudo-dynamic testing methods emerged. For these methods, the time scale between calculation and real-time operation converged, leading to real-time pseudo dynamic testing[9]. The main difference between HiL systems and real-time hybrid simulations is that the latter consists of an outer loop establishing a dynamic feedback loop based on the simulated and measured output.

In HiL systems, the physical prototype generates a force while the response of the physical prototype is generated in the numerical domain, involving a numerical solver, which can be implemented explicitly or implicitly. An explicit solver, on one hand, is relatively straightforward to implement and demands lower computational resources. On the other hand, an implicit solver is more complicated but offers the advantage of unconditional stability of the numerical model[5]. The numerical output is imposed on the physical structure by electrical or hydraulic actuators, which can be tailored to work for a single axis or multiple axes[10,11]. The loop introduces delays due to communication between the computer, servo-controller, and data acquisition systems[12]. Yet, it has been observed that the most critical source of delay is attributed to the actuator itself[13]. The concern arises from the phase shift between the numerical and actual responses, which results in a counterclockwise energy hysteresis, signifying an irreversible energy gain in the system, commonly referred to as negative damping[14]. If this accumulated energy leads to instability in the system, it can significantly reduce system performance and accuracy. To identify and predict instability of the system, a critical time delay can be formulated. This formulation is typically derived by solving the characteristic equations of delay differential equations, applicable to both single-degree-of-freedom representations of structures[15,16], and multi-degree-of-freedom representations of structures[17,18].

So far, hybrid testing techniques mainly have been applied in scenarios when the externally applied forces could be controlled; e.g. when predefined seismic events[19], waves[20–24], wind thrust and gusts[25–27], and fire[28,29] were applied. These examples show that the effect of the structural response on the external force was either zero or insignificant. For ice-induced vibrations, neither the force nor the forcing frequency can be predefined or accurately predicted—the system must consider highly non-linear and almost instantaneous frequency and magnitude variations in the loading (and thus response). Due to the unpredictability of the response, even small delays in the system could lead to a zero phase margin within the open loop and thus instability of the system.

The objective of this study was to analyze the robustness, performance and limitations of a test setup developed for Hardware-in-the-Loop simulations in model Ice (HiLI). An application of HiLI, which shows high robustness and performance, would introduce several advantages: properties of the offshore structure could be varied numerically; multi-degree-of-freedom representations of structures in ice could be investigated and multi-axial ice loading could be simulated. But most important, the method would allow to test structures, with relatively low natural eigenfrequencies as typical for heavy or tall offshore structures, like offshore wind turbines, in model ice experiments.

The study begins by introducing and explaining the HiL system developed. Next, 204 separate experiments, conducted during two model test campaigns[30,31], are investigated to analyze the robustness and performance of HiLI. Outliers are analyzed in further detail. Furthermore, the critical delay is determined experimentally and compared to an analytically derived delay. Finally, the results are discussed, and a conclusion is provided.

Method

Hardware-in-the-Loop testing

In the present study, the full offshore structure has been simplified during the Hardware-in-the-Loop experiments as illustrated in Fig. 1 with the example of an offshore wind turbine. The idea of the developed system was that only the small ice loaded strip of the full-scale structure is modelled physically. The mass of this strip is insignificant in comparison to the mass of the full-scale structure. It was thus decided to simplify the physical prototype to a rigid, geometrical interface that can crush the ice while providing insignificant damping and mass. Thus neither stiffness, mass, nor damping were assigned to the physical protoype and it became effectively a single point with negligible mass. The pile was manufactured from thin-walled aluminum to minimize the mass while deforming less than 10 micrometer under estimated maximum ice loading. Geometrical scaling effects caused by the choice of prototype geometry were analyzed in a separate study and were found to be minor[31]. The structural model and potential wind load were both handled numerically. Motion of the physical prototype was imposed by two electrical actuators. The hardware was mounted to a carriage of the Ice and Wave tank of the Aalto University. While it is feasible to push ice sheets against a stationary structure, the chosen approach was to move the entire test setup through a stationary ice sheet instead. This decision was influenced by the existing infrastructure of ice tanks, which are often tailored for maneuvering ship models through stationary ice sheets. Consequently, these ice tanks frequently feature a carriage designed to traverse rail systems along an ice channel or attached to a bridge which extends across an entire basin to allow for bi-directional movement. Utilizing a support frame (see Fig. 2a), the developed setup was affixed to the carriage of the tank and then moved through the ice as depicted in Fig. 2b. A narrow open channel can be seen in Fig. 2b as the physical prototype (i.e., the aluminum pile) crushes through the ice.

Hardware and numerics

The primary components of the hardware comprised three aluminum plates (Fig. 3). The upper plate was rigidly bolted to the carriage by installation of an additional support frame (Fig. 2a). In contrast, the two lower plates were capable of uni-directional movement, enabled by the installation of four caged roller linear motion guides. These guides were designed to minimize friction within the system. To further reduce the overall system mass

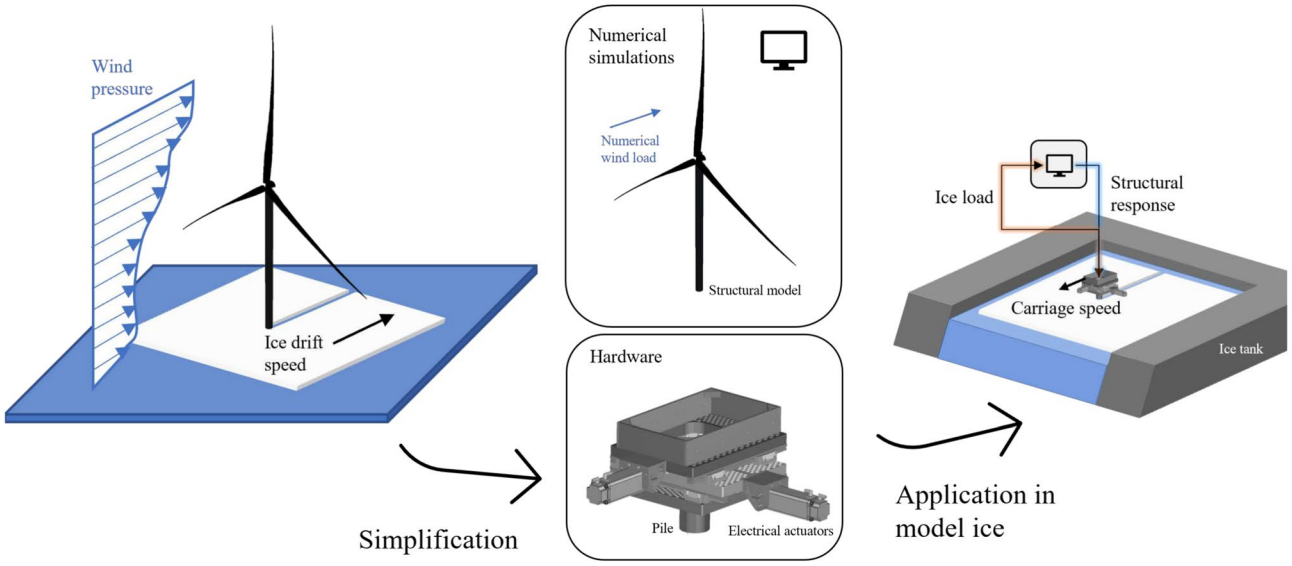

Figure 1. The full problem of an offshore wind turbine under wind and ice loading was simplified to a HiL system.

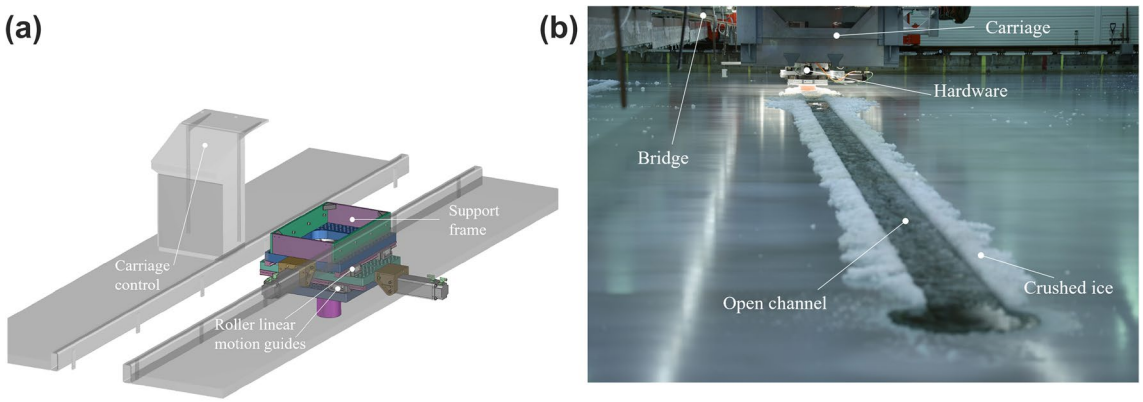

Figure 2. Application of a HiL system in model ice.

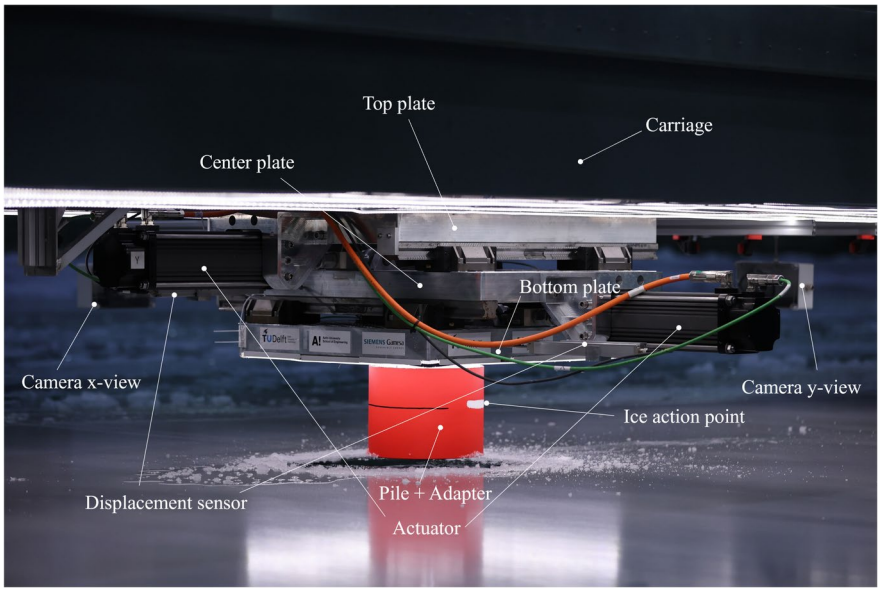

Figure 3. Photograph of the developed test setup during the second SHIVER model test campaign.

and subsequently lessen the inertial load experienced by the actuators and recorded by the implemented sensors for ice load identification, a honeycomb hollowing pattern was milled into the aluminum plates. This weight reduction also ensured compliance with the load limits of the carriage-bridge system.

The bi-axial displacements of the two lower plates were monitored using magnetostrictive displacement sensors (BIW0007-BIW1-A310-M0250-P1-S115, Balluff B.V., 5232 BC 's-Hertogenbosch, The Netherlands). Two different ice load measurement systems in combination with two different aluminum piles were employed during the development of the HiL system. In the first design, an aluminum pile featured two weakened rings to accommodate the installation of 16 strain gauges. This configuration allowed for the closest possible measurement of ice load to the waterline[32]. The second design utilized a shorter aluminum pile fitted with three load cells (2960-2962-2965 low-profile pancake load cells, SENSY S.A., 6040 Jumet, Belgium) at the flange of the pile (Fig. 4a). The shorter pile facilitated the use of 3D-printed adapters (Fig. 3), which allowed for the adjustment of the interface shape, diameter, and slope of the physical prototype. The application of 3D-printed materials for conducting ice crushing experiments was investigated in advance[33]. The specific ice load application heights (black line in Fig. 3) can be found in a separate study[31]. To capture the dynamics of the physical prototype, four accelerometers were strategically placed: one inside the pile (ADXL326, Analog Devices Inc., Wilmington MA 01887, USA) and one probe (ADXL327, Analog Devices Inc., Wilmington MA 01887, USA) each at the bottom, center, and top plate, as depicted in Fig. 4b. Additionally, axial load measurements were carried out at the connection point between the top plate and the transfer system (i.e., electrical actuators), utilizing VST5000 S-type load cells (HENK MAAS Weegschalen B.V., 4264 AW Veen, The Netherlands). This load measurement served for redundancy and verification of static load measurements. To document the setup from different angles, two cameras (GoPro Hero 9) were positioned to record video footage along each axis.

Two displacement-controlled electrical integrated motor actuators (GSX50-1005-MKR-SB5-358-G2, ACT UATION DIVISION—EXLAR Corporation, Eden Prairie MN 55346, USA) were installed. For computation, a Teensy USB Development Board (Version 3.6, PJRC) was utilized. During the experiments a PID controller (SD6 servo drive controller, STÖBER Antriebstechnik GmbH + Co. KG, Pforzheim, Germany) was used to enforce the boundary conditions. The verification of the functionality of the control system was carried out by replicating predefined displacement time series through the use of the actuators in dry test experiments[32]. During those experiments, the controller settings were tailored to each actuator separately to improve the overall performance[32]. No outer loop control was implemented. Within the carriage, both motors of the controller were situated. Additionally, the software and data acquisition were overseen and managed from this location. The carriage rode on twin rails and four dual bogies in total. The carriage was propelled by a rack-and-pinion system with two drive pinions.

Numerical simulations

The offshore structures were represented by linearized single- or multi-degree-of-freedom models in the modal domain. These models encompassed structural properties, including frequency, damping, and mass-normalized modal amplitudes in both the x- and y-direction at the point of ice action. The structural models were truncated and comprised structural frequencies up to 20 Hz to reduce the computational complexity and thus the internal simulation time. The value was also chosen as ice loads typically do not excite higher frequencies (see A.8.2.6.1.5[34]). Furthermore, the numerical model allowed for the application of external loads $F_{y;ext}$ and $F_{x;ext}$ at locations distinct from the ice action point, affecting the structural displacements in the x- and y-direction, respectively. For example, this facilitated the inclusion of wind loading at the tower top of an offshore wind turbine. The equations of motion in the modal domain are as follows:

$$\ddot{w}_i(t) + 2\zeta_i\omega_i\dot{w}_i(t) + \omega_i^2 w_i(t) = \begin{bmatrix}\phi_{i,x;ice} & \phi_{i,y;ice}\end{bmatrix}\begin{bmatrix}F_{x;ice}\\ F_{y;ice}\end{bmatrix} + \begin{bmatrix}\phi_{i,x;ext} & \phi_{i,y;ext}\end{bmatrix}\begin{bmatrix}F_{x;ext}\\ F_{y;ext}\end{bmatrix} \quad (1)$$

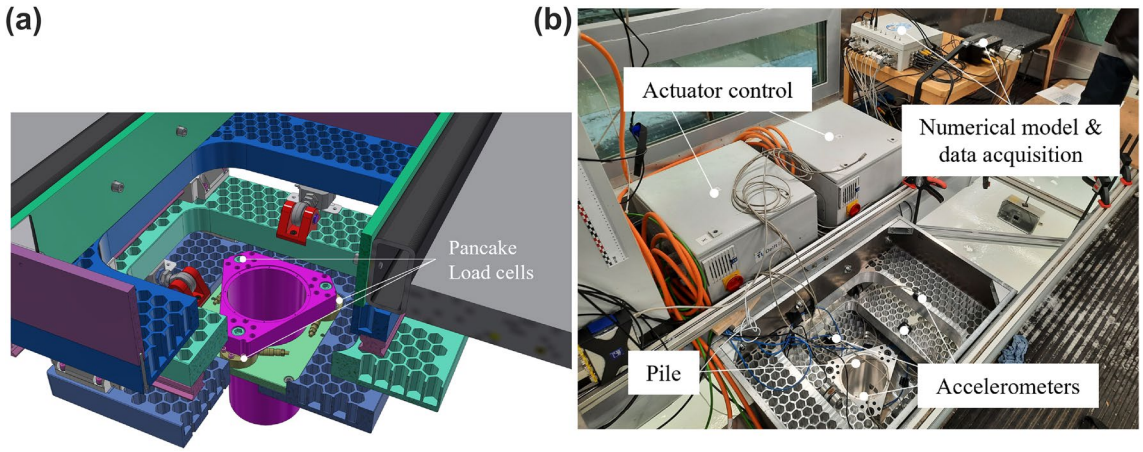

Figure 4. Visualization of the developed test setup for hybrid tests in model ice.

here, w_i represents the modal displacement of mode i, and the over-dots signify derivatives with respect to time. ζ_i denotes the damping ratio as a fraction of critical damping, and ω_i stands for the natural frequency. $\phi_{i,x;ice}$ and $\phi_{i,y;ice}$ are the mass-normalized modal amplitudes of mode i at the ice point and $\phi_{i,x;ext}$ and $\phi_{i,y;ext}$ on any other external point respectively, satisfying the equation:

$$\boldsymbol{\phi}_i^T \cdot \boldsymbol{M} \cdot \boldsymbol{\phi}_i = 1. \tag{2}$$

here, $\boldsymbol{M}$ refers to the mass matrix, and $\boldsymbol{\phi}_i$ represents the mass-normalized mode shape vector for mode i. Note that Eq. (1) does not consider any contribution of the physical prototype as the pile was designed to behave as a rigid interface of negligible mass to crush the ice. The prototype displacement at the water line d_y as measured by the displacement sensors at time t_j at iteration j shown in Fig. 3, is:

$$d_y(t_j) = x(t_j - \tau) \tag{3}$$

whereas

$$x(t_j) = \sum_{i=1}^{n} \phi_{i;x;ice} \cdot w_i(t_j); \tag{4}$$

τ is the delay between the output signal and the measured displacement. The equations were solved in each iteration j using the semi-implicit Euler–Cromer method with a time step size (Δt) of 10^{-4} s:

$$\ddot{w}_i(t_j) = \begin{bmatrix}\phi_{i;x;ice} & \phi_{i;y;ice}\end{bmatrix} \begin{bmatrix}F_{x;ice}(t_j) \\ F_{y;ice}(t_j)\end{bmatrix} + \begin{bmatrix}\phi_{i;x;ext} & \phi_{i;y;ext}\end{bmatrix} \begin{bmatrix}F_{x;ext}(t_j) \\ F_{y;ext}(t_j)\end{bmatrix} - 2\zeta_i\omega_i\dot{w}_i(t_j) - \omega_i^2 w_i(t_j) \tag{5}$$

with

$$\dot{w}_i(t_{j+1}) = \dot{w}_i(t_j) + \Delta t \cdot \ddot{w}_i(t_j) \tag{6}$$

and

$$w_i(t_{j+1}) = w_i(t_j) + \Delta t \cdot \dot{w}_i(t_{j+1}). \tag{7}$$

The execution time for the time-stepping function was approximately 55 µs for the structural model with the highest number of modes.

Constant delay compensation

After analysis of initial experiments in the ice tank, the delay τ between the measured pile position and position in the control system was quantified to be 4–5 ms. To address this delay, a constant delay compensation was implemented to predict the structural position forward by a time interval of Δt_{fp} equal to 5 ms:

$$\dot{w}_{i;\mathrm{fp}}(t_j) = \dot{w}_i(t_j) + \Delta t_{\mathrm{fp}} \cdot \ddot{w}_i(t_j) \tag{8}$$

$$w_{i;\mathrm{fp}}(t_j) = w_i(t_j) + \Delta t_{\mathrm{fp}} \cdot \dot{w}_{i;\mathrm{fp}}(t_j) \tag{9}$$

here, $w_{i;\mathrm{fp}}$ corresponds to the forward-predicted modal displacement. The forward-predicted output was generated by substitution of $w_{i;\mathrm{fp}}$ (Eq. 9) into Eq. (4) to compensate for the delay. Two simplified flow charts, illustrating the signal flow in the system, are presented in Fig. 5.

Scaling

The applied scaling method is explained in detail in a separate study[31]. However, a short summary is given here. The scaling method combines replica modeling and preservation of kinematics during testing. More specifically, the replica modeling results in a mean pressure similarity, while the preservation of kinematics denies any scaling of time components (either of the structure or of the ice). The mean pressure similarity allows to scale the numerical structural properties based on the ratio between a measured model-scale and an estimated full-scale mean ice load. For example, the numerical mass, stiffness and damping (m, k, c) are significantly but equally reduced when a large full-scale mean ice load (e.g., caused by a thick full-scale ice sheet) is tested. The damping ratio ζ and structural eigenfrequency f remain unchanged since both numerical stiffness and mass are scaled by the same factor.

In the next section, the robustness and performance of the HiLI is analyzed. It should be noted that the delay τ shown in the following two sections, if not stated otherwise, is the delay before application of the constant forward prediction.

Results

To assess the robustness and performance of the HiLI, the delay after compensation, the normalized root mean square error (RMSE), and the peak tracking error between the measured pile position and the position in the control system were calculated for 204 experiments, as illustrated in Fig. 6. Notably, the developed setup demonstrated robust performance, with the majority of experiments showing a delay after compensation with a constant forward predicted time interval of approximately 0 to −0.5 ms, a normalized RMSE $< 0.6\%$, and a peak tracking error $< 1\%$, even when numerous parameters, such as the numerical structure, measurement system, physical

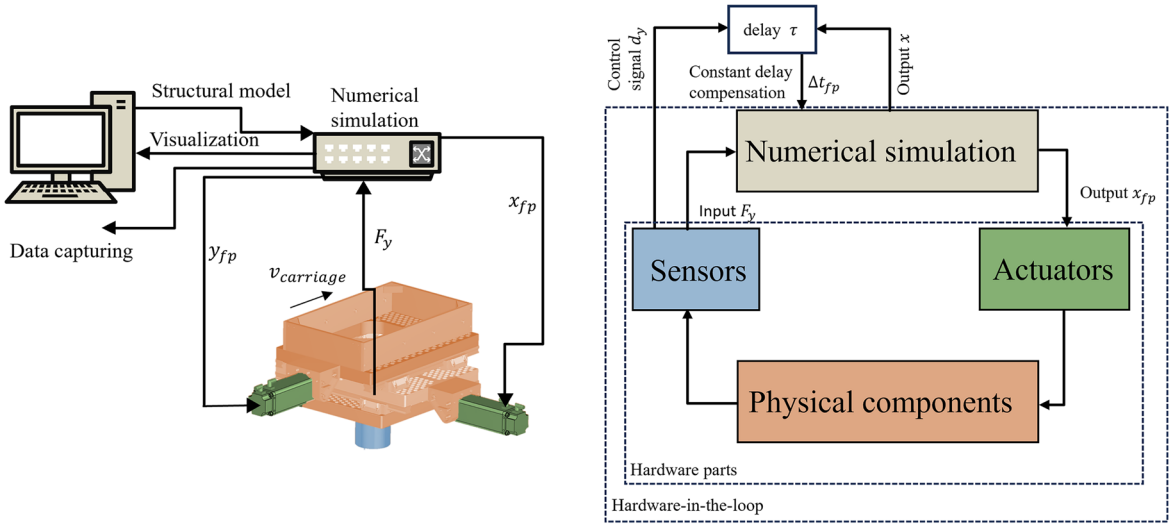

Figure 5. Signal flow charts illustrating the signal flow of the HiL simulations. The box flow chart has been adapted from the literature[35].

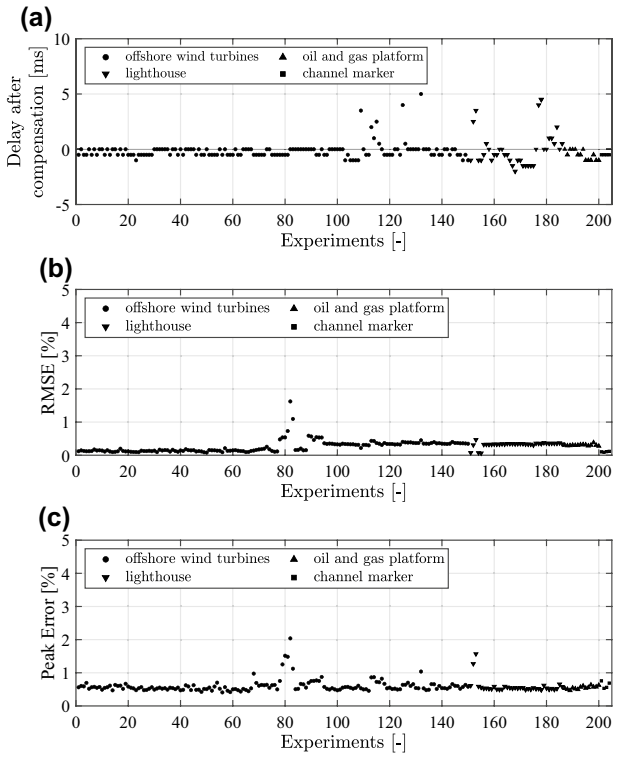

Figure 6. Performance parameters for 204 HiLI experiments.

prototype or ice type were altered. Note that the negative delay can be explained by the application of a constant delay compensation ($\Delta t_{\mathrm{fp}} = 5$ ms). The delay was calculated by identifying the maximum cross-correlation between the measured displacement and the output signal of the numerical model. To mitigate static fluctuations, a moving mean incorporating 4000 data points was applied, meaning that the average was subtracted for bins of 2 s as the sampling rate during the experiments was set to 2 kHz. The RMSE and peak tracking error were calculated as J2 and J3 in a benchmark control problem for real-time hybrid simulations[36].

However, exceptions in the data set were observed, where some experiments resulted in delays exceeding 0 ms as can be seen in Fig. 6a. These exceptions indicate that the stability of the system was not unconditional for all experiments. It was found that the outliers in Fig. 6 could be categorized into two distinct groups. The first group of exceptions (Experiments 132, 177–187) was linked to warm model ice tests. In warm model tests, the mean model ice load was significantly lower than during cold model tests. Measured loads of small magnitude,

induced by background vibrations (e.g, caused by the motor of the actuator), consequently started to affect the ice load identification. Thus, it is assumed that the high critical delays were caused by the low signal-to-noise ratio, an effect which can lead to undesired performance of hybrid tests[5]. The second group was associated with experiments simulating harsh ice conditions (i.e., scaling for a higher full-scale mean ice load) for a lighthouse structure (Experiments 113–117, 125–126) and offshore wind turbines (Experiments 152–153).

Results for the normalized root mean square error and peak tracking error are shown in Fig. 6b,c. Here two groups of outliers can be identified. The first group is related to experiments that also resulted in outliers in Fig. 6a (Experiments 152, 153). The second group is related to experiments of a smaller and thus stiffer offshore wind turbine (Experiments 78–83). These experiments did not result in a large delay of the HiLI. The error only manifested at higher test speeds, amplifying with each incremental rise in test velocity. It is assumed that the errors increased as one of the eigenfrequencies of that particular numerical structure was similar to the eigenfrequency of the carriage ($\sim$ 3.5 Hz). However, the magnitudes of both errors are still insignificant (RMSE $<$ 2%, Peak tracking error $<$ 2.1%), which is why the following analysis focuses on the outliers found for the delay in Fig. 6a.

One example of instability for a lighthouse experiment is shown in Fig. 7. Notably, delays of 10–12 ms were observed upon the initiation of the HiL system in open water when a numerical model of a lighthouse was implemented. Exponential growth in the measured "ice load" and structural displacement can be observed, particularly in the vicinity of a frequency close to 40 Hz. Note that the "ice load" in open water is initiated by small load amplitudes and measured inertia of the pile. This frequency is in the range of the natural frequency of the physical prototype, as a power spectral density of the measured pile accelerations during a separate rigid indentation experiments in Fig. 8 shows. Interestingly, once the aluminum pile was dragged through the ice for the lighthouse test ($t > 299$ s in Fig. 7), the delay in the HiLI decreased by approximately 25%. Simultaneously, the occurrence of high-frequency load and response reduced significantly. After all, it seems that once the physical prototype was in contact with the ice, the coupled system was less prone to instabilities. The physical prototype being in contact or not in contact with the ice could also explain the two highest peaks ($f_1 = 37.9$ and $f_2 = 43.4$ Hz) in the frequency swarm of the pile acceleration as shown in Fig. 8. The effect of ice-structure coupling on the overall HiLI stability is further discussed in "Ice-structure coupling".

Another experiment from the second outlier group (i.e., experiments aiming to test harsh ice conditions) resulting in a significant delay is depicted in Fig. 9. This figure illustrates an experiment of an offshore wind turbine simulation under harsh ice conditions. When compared to the time series of the lighthouse experiment shown in Fig. 7, the offshore wind turbine exhibited vibrations with a frequency close to 20 Hz. Only towards the end of the experiment did the vibration frequency converge to the eigenfrequency of the physical prototype, approximately in the range of 30–40 Hz. However, the experiment was prematurely terminated to prevent damage to the equipment. It remains a matter of speculation why the offshore wind turbine, scaled for harsh ice conditions, experienced vibrations at a frequency slightly higher than the highest numerically modeled eigenfrequency,

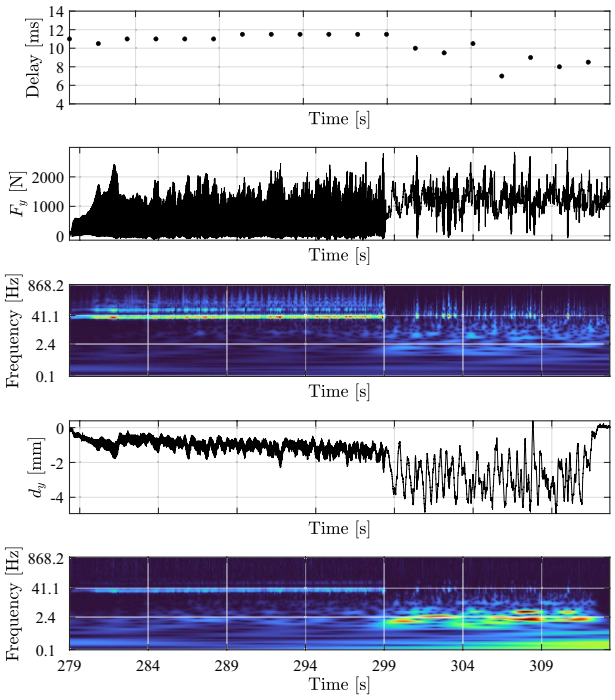

Figure 7. Measured delay during an experiment of a lighthouse scaled for harsh ice conditions. Additionally, time series and corresponding wavelet transformation of the measured ice load F_y and structural displacement d_y are shown. The setup first moves through open water (279–299 s) and then crushes through the model ice (299–313 s). Test ID 451[30].

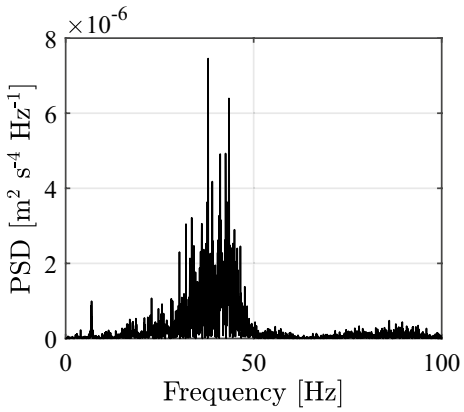

Figure 8. Power spectral density of the measured acceleration inside of the pile during a rigid indenter experiments through the ice. Test ID 514.

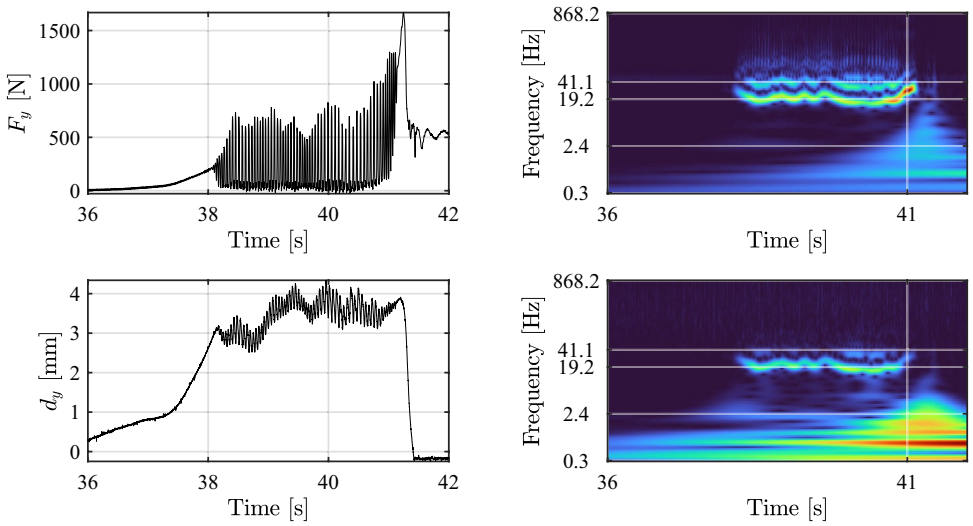

Figure 9. Results of HiLI when a numerical model of an offshore wind turbine was scaled for harsh ice conditions and implemented. Test ID 241.

whereas the experiment with a model of a lighthouse resulted in vibrations with a frequency equal to that of the physical prototype. One possible explanation is based on the fact that the highest natural eigenfrequency of the offshore wind turbine is higher than any modeled eigenfrequency of the lighthouse, and thus more prone to excitation by high frequency loads.

In summary, the majority of the experiments demonstrated delays that were either shorter or equal to the time increment applied in the constant forward prediction method. However, a few instances of larger delays were attributed to low signal-to-noise ratios and scaling of the numerical structures. Since the reasons for the instabilities resulting from the scaling for harsh ice conditions remain unclear, the subsequent investigation will focus on exploring the critical delays of the implemented numerical structures for such scenarios.

Critical delay

To explore the reasons behind certain numerical representations of structures becoming unstable while others remain stable, the critical delay was experimentally identified. The critical delay is the threshold beyond which a system accumulates more energy than it can dissipate. Subsequently, efforts were made to seek an analytical solution for this critical delay.

Experimental critical delay

Identifying a critical delay experimentally was a challenging task due to the need to test a range of numerical structure models, passing the transition from unstable to stable (or vice versa) HiLI. This transition was crucial to approximate a critical delay experimentally. As such, experiments were conducted with numerical models of a lighthouse and two offshore wind turbines, incrementally lowering the numerical stiffness and mass, equivalent to scaling for harsher ice conditions until HiLI instability was observed.

Next, experimental results of structures scaled for nine different full-scale ice mean loads are shown. Before testing, the implemented numerical model of a lighthouse was scaled to the ice mean load respectively. Each numerical structural model was tested in a separate experiment, resulting in one measured delay per 'Structure' (Fig. 10). Experiments that resulted in a delay exceeding 5 ms are highlighted in orange. The delay was identified based on the maximum cross-correlation between the measurement of the pile position and the equivalent value in the control system. Prior to cross-correlation, the quasi-static component of the time series was removed by subtracting the moving mean for a window of 2000 data points. The final experimental critical delay was obtained by subtracting the forward-predicted time (5 ms) from the experimental delay for unstable experiments. However, it is evident that the critical delay can only be approximated when the HiLI approaches the threshold of instability by this method, and yields an overestimation in other cases. On the threshold of instability, Structure 6 in Fig. 10 exhibited a delay of 8.5 ms. The actual critical experimental delay is thus 3.5 ms. Furthermore, two offshore wind turbines were experimentally tested, scaling two structures for each turbine type, identifiying the critical delay of those two offshore wind turbine types respectively (see Table 1).

Analytical critical delay

For evaluation of the experimentally identified critical delays, the authors chose to apply an analytical instability criterion formulated by[15]:

$$\omega_n \tau \frac{k_s}{k} < 2\zeta. \tag{10}$$

In this inequality, the stiffness k_s represents the stiffness of the physical test setup and is assumed to be constant for the time being. τ is the delay of the system, ω_n, k and ζ are numerical model parameters, namely the natural frequency, stiffness and damping ratio respectively. It is apparent that the left-hand side (LHS) of Eq. (10) increases as numerical structural stiffness decreases. When the LHS surpasses the right-hand side (RHS), the real parts of the solution for characteristic equation of the delay differential equation becomes positive, leading to a condition of instability[15]. Notably, Eq. (10) is based on the assumption that the eigenvalues remain complex as $\omega_n \tau$ is assumed to be small as $\tau \ll 1$, and thus only the real parts of the eigenvalues determine the overall stability. In other words, the system becomes unstable once τ_{crit} is reached:

$$\tau = \begin{cases} \tau & \omega_n \tau \frac{k_s}{k} < 2\zeta \\ \tau_{crit} & \omega_n \tau \frac{k_s}{k} = 2\zeta \end{cases} \tag{11}$$

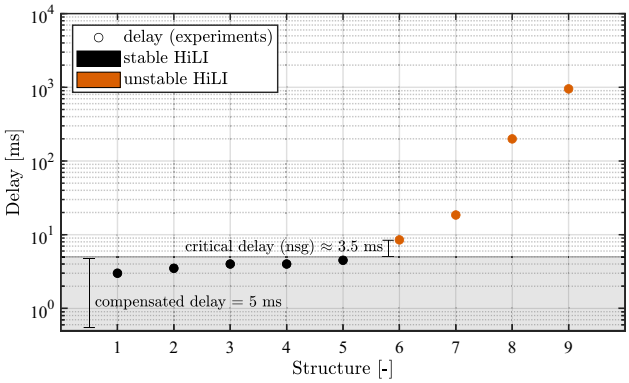

Figure 10. Experimental results for implemented numerical models of the lighthouse (nsg) scaled for nine different ice conditions from mild to severe. Test ID 81, 87, 84, 534, 533, 532, 531, 529, 530.

Structure	Test ID	Critical delay	
		Experimental (ms)	Analytical (ms)
Lighthouse	532	3.5	3.7
NREL OWT	241	2.0	2.3
Reference OWT	242	1.0	0.5
Oil and gas platform	(126)	–	<36
Channel marker	(554[30])	–	< 0.5

Table 1. Critical delays of investigated offshore structures. The parentheses indicate that only the structural models of these test IDs have been used to calculate the analytical critical delay—no experiments were performed.

It should be noted that the criterion was derived for a single-degree-of-freedom structural representation, which is why the coupling of the mode shapes via the forcing term for multi-degree-of-freedom structures is not captured in this analysis. First, the analytical critical delay was calculated based on Eq. (11) for the structures that were used to approximate an experimental critical delay. Thereby, the stiffness of the physical prototype k_s was computed using the natural frequency obtained from accelerometer measurements (Fig. 8). For calculation of the critical delay, the second peak of ($f_2 = 43.4$ Hz) was utilized as it was assumed to be the coupled frequency between structure and ice. This assumption is discussed in "Ice-structure coupling". The mass of the physical prototype (i.e., aluminum pile) was specified as 5 kg. The analytical solution yielded a critical delay of 3.7 ms for the lighthouse, 2.3 ms for the NREL (National Renewable Energy Laboratory) offshore wind turbine and 0.5 ms for a reference offshore wind turbine respectively. The close match between the critical delays and the experimental results, as shown in Table 1, is remarkable, especially considering that the experimental delay can only be approximated. The analytical critical delay was computed for every structural mode of each individual structural model. However, for clarity, only the smallest calculated value is presented here, as this value corresponds to the point at which the first shift in stability occurs. As the critical delay matches well with the experimental delay for which instability was observed, the criterion is also used to estimate the critical delays of the numerical representations of an oil and gas platform and a channel marker, which had been tested during the two test campaigns.

Due to their unique combination of structural properties, offshore wind turbines and the tested channel marker are predisposed to exhibit instability during HiLI. When scaling numerical structure models for harsh ice conditions, the interplay between low numerical stiffness and high numerical mass places the system in a precarious state close to instability. Minor perturbations during the experiments can trigger system instability, manifesting as high-frequency vibrations that impose substantial accelerations on the actuators, resulting in an increase in the measured delays. HiLI with a numerical model of the channel marker implemented were not seen to result in instability as the numerical models were scaled only for relatively mild ice conditions during the experiments.

Mitigation of instabilities

Experiments involving numerical models of offshore structures scaled for harsh sea ice conditions regularly resulted in HiLI instability. To mitigate such occurrences, three general measures can be implemented.

First, experiments can be conducted with a larger model-scale mean ice load, which reduces the scaling factor (the ratio between full-scale and model-scale mean ice load). This, in turn, results in less downscaling of the numerical stiffness, increasing the critical delay. Achieving a larger model-scale mean ice load can be accomplished by increasing the compressive strength of the model ice, installing a physical prototype with a larger projected width or increasing the ice thickness. However, the challenge of this approach is that very high loads cannot be accommodated without compromising the control systems or structural integrity of the test facilities. Second, the numerical (modal) representation of the offshore structures can be truncated to enhance stability[37]. While this approach involves modifying the original numerical model, it has proven effective in cases where the critical delay was primarily affected by higher structural modes. Truncating these modes eliminates instability and increases the critical delay. Alternatively, the propensity for higher structural mode instability can be mitigated by applying supplementary modal damping to the identified critical modes[38]. Third, various control methods are available to alleviate and offset time delays, including techniques such as nominal extrapolation, phase-lead compensation, model-based compensation, derivative feed-forward, inverse compensation, virtual coupling, smith regulator, fuzzy logic, three variable control, infinite impulse response, impedance matching, passivity-based or adaptive compensation. For a more comprehensive understanding of these methods, a detailed explanation can be found in the work of Palacio-Betancur and Soto[5].

By combining all three measures (1: scaling for higher mean load, 2: truncating the numerical model, 3: constant delay compensation), stable HiLI simualting the NREL offshore wind turbine in harsh sea ice have been achieved (Fig. 11). The same numerical offshore wind turbine model as in Fig. 9 was used, which resulted instantly in instability and led to an abortion of the experiment. But now, the numerical structure model was truncated and the numerical structural properties were scaled for a slightly higher mean model ice load.

Discussion

Ice-structure coupling

In the preceding analysis, the stiffness of the physical prototype, denoted as k_s, was presumed to remain constant. However, an examination of the time series from an experiment with a numerical representation of a lighthouse scaled to emulate harsh sea ice conditions (Fig. 7), raised the question if the stiffness of the physical prototype during testing was inherently constant.

The clear differentiation between the two phases of critical delays in Fig. 7 suggests that the delay reduction is likely linked to the physical coupling of the ice to the physical prototype, effectively increasing the stiffness of the coupled physical prototype ($k_{s;\text{coupled}}$). The two highest peaks observed in the frequency swarm of the measured pile acceleration (Fig. 8) provide support for this hypothesis: a 25% reduction in the delay τ, when expressed in Eq. (11) while other variables remain constant, implies a proportionate increase in the stiffness of the coupled physical prototype ($k_{s;\text{coupled}}$). Given the insignificance of the mass of the model ice, the coupled eigenfrequency of the physical prototype would be roughly 15% higher than the eigenfrequency of the physical prototype when not in contact with the ice. Notably, the two frequencies of maximum PSD in the acceleration signal (Fig. 8) differ by exactly 15%. The same difference can also be found when the measured frequency (≈ 20 Hz) in (Fig. 9) is compared to the highest modelled frequency of 17.31 Hz. Therefore, it is reasonable to surmise that the eigenfrequency of the physical prototype when coupled to the ice was $\omega_{s;\text{coupled}} = f_2 = 43.4$ Hz, while otherwise, $\omega_{s;\text{uncoupled}} = f_1 = 37.9$Hz. However, the swarm of frequencies in Fig. 8 also shows that the contact

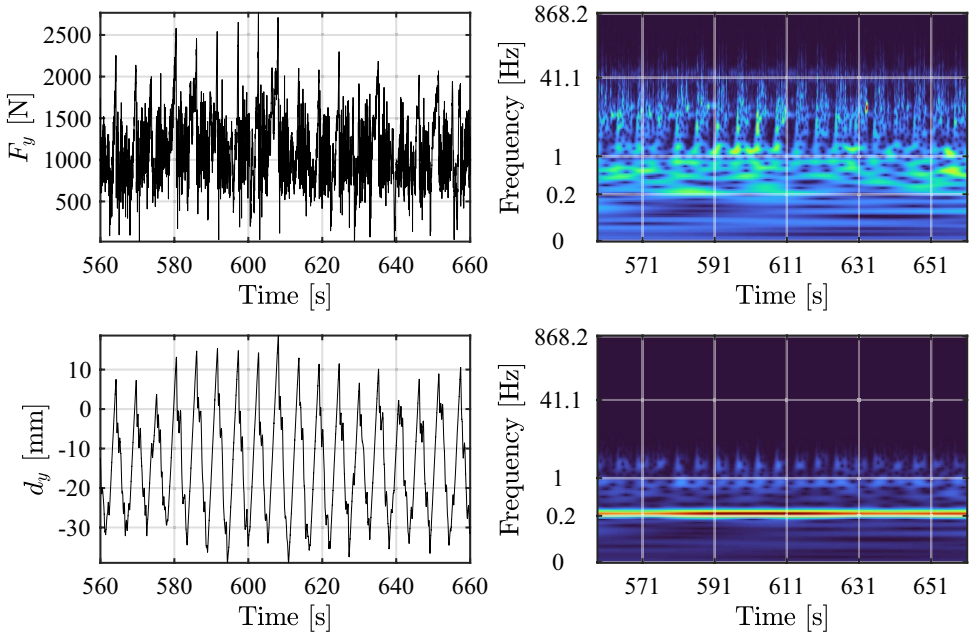

Figure 11. Stable HiLI for a numerical model of an offshore wind turbine scaled for harsh ice conditions. Test ID 498.

is not binary. The ice-structure contact is time varying and thus is the PSD. Nevertheless, it can be stated that the coupling between the physical prototype and ice reduces the delay of the system by increasing the coupled stiffness of the physical prototype during ice-structure interaction. The ice acted as a natural measure to mitigate the instability of the HiLI when in contact with the prototype.

Applicability

The developed setup enables to perform HiLI for analysis of offshore structures subjected to crushing ice conditions. However, our analysis has unveiled certain limitations associated with these simulations. We observed that the approach adopted led to instability of HiLI when a combination of harsh ice conditions and flexible numerical representations of structures were investigated. While this clearly imposes a constraint on HiLI, it is worth noting that the combination of a flexible structure and severe ice conditions is unlikely to occur in reality, as design for such conditions would typically result in stiff offshore structures to be able to satisfy design requirements in standards. There is also room for debate about whether such stiff offshore structures should still be represented by a multi-degree of freedom model, as high frequencies might not be excited and, consequently, may not be a concern for the offshore structure design. The application of HiLI involves a trade-off between achieving physical accuracy and considering design constraints. For example, in the context of offshore wind turbines, it remains crucial to include higher structural modes in the numerical domain. However, when scaling the numerical model of an offshore wind turbine for harsh ice conditions, higher structural modes are prone to instability. Additionally, structural frequencies close to the eigenfrequency of the carriage should be excluded from the numerical structural models, as severe carriage vibrations were observed in such experiments, which supposedly negatively affected the RMSE and peak tracing error. Over the course of two test campaigns, single-degree- and multi-degree-of-freedom structural representations with frequencies ranging from 0.15 to 17.31 Hz were successfully tested. Models of offshore wind turbines were examined under full-scale ice loads of approximately 2.2 MN in mild ice conditions and around 7.8 MN in harsh ice conditions. For harsh ice conditions, stable HiLI were only achieved by implementing a truncated structural model of the stiffer NREL offshore wind turbine at increased model-scale mean ice loads. HiLI with structural representations of lighthouses implemented, were successfully tested for ice loads ranging from mild to severe ice conditions ($\approx$ 0.4 to 2–4 MN). The highest full-scale ice load scaled for was 75 MN for an oil and gas platform. The application of HiLI allowed to investigate ice-structure interaction of offshore structures like offshore wind turbines[39–42], lighthouses[31], oil and gas platforms[31], and channel markers. With the numerical model deactivated, the developed test setup functioned as a rigid indenter for a range of constant ice velocities from 0.0001 to 0.5 m/s to study velocity effects on structures[31]. Additionally, ramped, harmonic, and haversine velocity profiles could be investigated in forced vibration experiments[43]. The possibility to install modular 3D-prints enabled to vary structural diameter, shape, and slope of the physical prototype to investigate aspect ratio and shape effects on the development of ice-induced vibrations during the second test campaign[31].

In summary, the versatility of the HiLI allows for the coverage of a wide spectrum of level ice scenarios in mild conditions, while addressing more severe ice conditions may require the application of methods to mitigate the risk of HiLI instability. Physical substructural diameters were constrained to a low ratio between diameter and

model ice thickness which prevented model ice buckling. It is important to note that the HiLI were performed with a specific focus on ice-structure interaction and ice-induced vibrations, which implies crushing failure of ice for which good results were obtained. HiLI may not be suitable for investigating ice load scenarios exceeding those encountered in harsh ice conditions. For example, it seems questionable if ridge ice loads acting on an offshore wind turbine could be simulated without experiencing instabilities of the HiLI. But before experimentally delving into ridge loads for slender structures, it is imperative to gain a comprehensive understanding of whether dynamic ice-structure interactions should be considered in such scenarios. Our test setup lacks the capability to handle horizontal ice loads when significant vertical loads are present, as the horizontal ice load identification process disregarded the vertical components to solve the over-determined load measurement system. Furthermore, it is unknown how the HiLI perform when ice loads, stemming from an ice action event with a significantly varying (or unknown) ice action point, are considered (e.g. during ice bending or for 'thick' ice). This limitation arises from the implementation of a static arm for horizontal load identification. To fully capture the acting forces, it would be necessary to employ a 6-DOF load cell or to develop a compensation algorithm for determining the variation in the static ice load through numerical means.

Conclusion

Prior to this study, hybrid testing techniques, such as Hardware-in-the-Loop testing, had not been explored for investigating the ice-structure interaction of offshore structures, with relatively low natural frequencies, and drifting sea ice. The need for such techniques stems from challenges associated with the scaling for dynamic ice-structure interaction and exceeding capacities of test facilitates when testing of offshore structures like offshore wind turbines is required. The present study elaborated on the developed hybrid test setup and presented the implemented constant delay compensation. 204 experiments were analyzed to evaluate the robustness and stability of Hardware-in-the-Loop simulations in model ice (HiLI) under various conditions. It was only in cases where numerical structural properties were adjusted to accommodate substantial full-scale mean ice loads that the observed delays exceeded the critical thresholds. The large delay prompted the development of instability as confirmed by analyzing the time series of load and structural response. The performance of HiLI also reduced when model ice, that resulted in significant lower mean ice loads, was tested, as a low signal-to-noise ratio emphasized the presence of background noises. Furthermore, it was found that the stiffness of the physical prototype was changing significantly due to the interaction with the ice. During periods of ice crushing, HiLI resulted in reduced delays and hence a lower likelihood of becoming unstable. Thus, ice-structure coupling led to a mitigation of instability of HiLI by increasing the physical prototype stiffness. Finally, critical delays were experimentally determined and confirmed by a simplified analytical solution, substantiating the assumption that the reduction in the numerical stiffness caused the instabilities of the HiLI. However, testing with higher model-scale mean ice loads and truncation of the numerical structural models improved the stability of HiLI and allowed to run stable experiments of an offshore wind turbine under harsh ice conditions.

In summary, the applied hybrid testing technique (i.e., HiLI) demonstrated robust and stable simulations of offshore wind turbines, lighthouses, oil and gas platforms, and channel markers in model ice tank experiments aimed at capturing ice-induced vibrations due to crushing of ice. The developed hybrid setup allowed to maintain the full-scale structural eigenfrequencies and structural displacements of offshore structures, while enhancing versatility in adjusting structural properties and substructural shapes to investigate the dependency of structural properties, shape and aspect ratio on the development of ice-induced vibration regimes. The present study hopefully lays the foundation for a broader application of hybrid testing techniques in model ice experiments.

Data availability

The full experimental data set can be obtained upon request from Tim C. Hammer (T.C.Hammer@tudelft.nl). A condensed data set (excluding data for Fig. 6) can be obtained here: https://data.4tu.nl/datasets/be53fc9d-3d5a-4aee-b694-cd92c66e6403/1.

Received: 25 January 2024; Accepted: 30 July 2024
Published online: 07 August 2024

References

1. Hendrikse, H. Dynamic ice actions in the revision of ISO 19906. In *Proceedings of the 25th International Conference on Port and Ocean Engineering under Arctic Conditions* (2019).
2. Määttänen, M. Dynamic ice-structure interaction during continuous crushing. Tech. Rep., U.S. Army Cold Regions Research and Engineering Laboratory, Hanover, New Hampshire, USA (1983).
3. Ziemer, G. & Evers, K.-U. Model tests with a compliant cylindrical structure to investigate ice-induced vibrations. *J. Offshore Mech. Arctic Eng.*https://doi.org/10.1115/1.4033712 *(2016).*
4. Hendrikse, H., Ziemer, G. & Owen, C. C. Experimental validation of a model for prediction of dynamic ice-structure interaction. *Cold Regions Sci. Technol.* **151**, 345–358. https://doi.org/10.1016/j.coldregions.2018.04.003 (2018).
5. Palacio-Betancur, A. & Gutierrez Soto, M. Recent advances in computational methodologies for real-time hybrid simulation of engineering structures. *Arch. Comput. Methods Eng.* **30**, 1637–1662 (2023). https://doi.org/10.1007/s11831-022-09848-y.
6. Hakuno, M., Shidawara, M. & Hara, T. Dynamic destructive test of a cantilever beam, controlled by an analog-computer. in *Proceedings of the Japan Society of Civil Engineers*, 1–9 (1969).
7. Takanashi, K., Udagawa, K., Seki, M., Okada, T. & Tanaka, H. Non-linear earthquake response analysis of structures by a computer-actuator on-line system. *Trans. Arch. Inst. Jpn.* **229**, 1–17. https://doi.org/10.3130/aijsaxx.229.0 (1975).
8. Takanashi, K. & Ohi, K. Earthquake response analysis of steel structures by rapid computer-actuator on-line system. *Trans. Arch. Inst. Jpn.* 103–109 (1983).
9. Nakashima, M., Kato, H. & Takaoka, E. Development of real-time pseudo dynamic testing. *Earthq. Eng. Struct. Dynam.* **21**, 79–92. https://doi.org/10.1002/eqe.4290210106 (1992).
10. Bonnet, P. A. *The Development of Multi-Axis Real-Time Substructure Testing*. Ph.D. thesis, University of Oxford (2006).

11. Najafi, A., Fermandois, G. A. & Spencer, B. F. Decoupled model-based real-time hybrid simulation with multi-axial load and boundary condition boxes. *Eng. Struct.*https://doi.org/10.1016/j.engstruct.2020.110868 *(2020).*
12. Carrion, J. E. & Spencer, B. F. Model-based Strategies for Real-time Hybrid Testing. Tech. Rep. January 2007, University of Illinois at Urbana-Champaign (2007).
13. Zhao, J., French, C., Shield, C. & Posbergh, T. Considerations for the development of real-time dynamic testing using servo-hydraulic actuation. *Earthq. Eng. Struct. Dynam.* **32**, 1773–1794. https://doi.org/10.1002/eqe.301 (2003).
14. Horiuchi, T., Inoue, M., Konno, T. & Namita, Y. Real-time hybrid experimental system with actuator delay compensation and its application to a piping system with energy absorber. *Earthq. Eng. Struct. Dynam.* **28**, 1121–1141 (1999). https://doi.org/10.1002/(SICI)1096-9845(199910)28:10<1121::AID-EQE858>3.0.CO;2-O
15. Wallace, M. I., Sieber, J., Neild, S. A., Wagg, D. J. & Krauskopf, B. Stability analysis of real-time dynamic substructuring using delay differential equation models. *Earthq. Eng. Struct. Dynam.* **34**, 1817–1832. https://doi.org/10.1002/eqe.513 (2005).
16. Zhou, H., Shao, X., Zhang, B., Tan, P. & Wang, T. Relative stability analysis for robustness design of real-time hybrid simulation. *Soil Dynam. Earthq. Eng.* **165**, 107681. https://doi.org/10.1016/j.soildyn.2022.107681 (2023).
17. Maghareh, A., Dyke, S., Rabieniaharatbar, S. & Prakash, A. Predictive stability indicator: A novel approach to configuring a real-time hybrid simulation. *Earthq. Eng. Struct. Dynam.*https://doi.org/10.1002/eqe *(2016).*
18. Gao, X. S. & You, S. Dynamical stability analysis of MDOF real-time hybrid system. *Mech. Syst. Signal Process.* **133**, 106261. https://doi.org/10.1016/j.ymssp.2019.106261 (2019).
19. McCrum, D. P. & Williams, M. S. An overview of seismic hybrid testing of engineering structures. *Eng. Struct.* **118**, 240–261. https://doi.org/10.1016/j.engstruct.2016.03.039 (2016).
20. Thys, M. *et al.* Real-time hybrid model testing of a semi-submersible 10MW floating wind turbine and advances in the test method. In Proceedings of the *ASME 2018 1st International Offshore Wind Technical Conference, IOWTC 2018*. https://doi.org/10.1115/IOWTC2018-1081 (2018).
21. Luan, C., Gao, Z. & Moan, T. Comparative analysis of numerically simulated and experimentally measured motions and sectional forces and moments in a floating wind turbine hull structure subjected to combined wind and wave loads. *Eng. Struct.* **177**, 210–233. https://doi.org/10.1016/j.engstruct.2018.08.021 (2018).
22. Sun, C., Song, W. & Jahangiri, V. A real-time hybrid simulation framework for floating offshore wind turbines. *Ocean Eng.* **265**, 112529. https://doi.org/10.1016/j.oceaneng.2022.112529 (2022).
23. Bachynski, E. E., Thys, M., Sauder, T., Chabaud, V. & Sæther, L. O. REAL-TIME HYBRID MODEL TESTING OF A BRACELESS SEMI-SUBMERSIBLE WIND TURBINE. PART II: EXPERIMENTAL RESULTS. In *Proceedings of the ASME 2016 35th International Conference on Ocean, Offshore and Arctic Engineering*, 1, 1–12 (Busan, South Korea, 2016).
24. Sauder, T., Chabaud, V., Thys, M., Bachynski, E. E. & Sæther, L. O. REAL-TIME HYBRID MODEL TESTING OF A BRACELESS SEMI-SUBMERSIBLE WIND TURBINE. PART I: THE HYBRID APPROACH. In *Proceedings of the ASME 2016 35th International Conference on Ocean, Offshore and Arctic Engineering*, 1–13 (Busan, South Korea, 2016).
25. Ruffini, V., Szczyglowski, C., Barton, D. A., Lowenberg, M. & Neild, S. A. Real-time hybrid testing of strut-braced wing under aerodynamic loading using an electrodynamic actuator. *Exp. Tech.* **44**, 821–835. https://doi.org/10.1007/s40799-020-00394-5 (2020).
26. Wu, T. & Song, W. Real-time aerodynamics hybrid simulation: Wind-induced effects on a reduced-scale building equipped with full-scale dampers. *J. Wind Eng. Ind. Aerodynam.* **190**, 1–9. https://doi.org/10.1016/j.jweia.2019.04.005 (2019).
27. Zhang, Z., Basu, B. & Nielsen, S. R. Real-time hybrid aeroelastic simulation of wind turbines with various types of full-scale tuned liquid dampers. *Wind Energy* **22**, 239–256. https://doi.org/10.1002/we.2281 (2019).
28. Wang, X., Kim, R. E., Kwon, O.-S., Yeo, I.-H. & Ahn, J.-K. Continuous real-time hybrid simulation method for structures subject to fire. *J. Struct. Eng.* **145**, 1–12. https://doi.org/10.1061/(asce)st.1943-541x.0002436 (2019).
29. Mergny, E. & Franssen, J. M. Multi-degree-of-freedom hybrid fire testing of a column in a non-linear environment. *Fire Technol.*https://doi.org/10.1007/s10694-022-01258-7 *(2022).*
30. Hendrikse, H. *et al.* Experimental data from ice basin tests with vertically sided cylindrical structures. *Data Brief* **41**, 1–18. https://doi.org/10.1016/j.dib.2022.107877 (2022).
31. Hammer, T. C., Puolakka, O. & Hendrikse, H. Scaling ice-induced vibrations by combining replica ice modeling and preservation of kinematics. *Cold Regions Sci. Technol.*https://doi.org/10.1016/j.coldregions.2024.104127 *(2024).*
32. Hammer, T. C., Beek, K. V., Koning, J. & Hendrikse, H. A 2D test setup for scaled real-time hybrid tests of dynamic ice- structure interaction. in *Proceedings of the 26th International Conference on Port and Ocean Engineering under Arctic Conditions*, 1–13 (POAC, Moscow, Russia, 2021).
33. Petry, A., Hammer, T. C., Hendrikse, H. & Puolakka, O. Ice basin experiments on mixed-mode failure on ice cones. in *Proceedings of the 27th International Conference on Port and Ocean Engineering under Arctic Conditions* (POAC, Glasgow, UK, 2023).
34. ISO 19906:2019(E). Petroleum and natural gas industries—Arctic offshore structures (2019).
35. Lee, C. & Tu, J. Y. Preliminary comparison of hybrid testing techniques. *Procedia Eng.* **79**, 490–494. https://doi.org/10.1016/j.proeng.2014.06.370 (2014).
36. Silva, C. E., Gomez, D., Maghareh, A., Dyke, S. J. & Spencer, B. F. Benchmark control problem for real-time hybrid simulation. *Mech. Syst. Signal Process.* **135**, 106381. https://doi.org/10.1016/j.ymssp.2019.106381 (2020).
37. Miraglia, G., Petrovic, M., Abbiati, G., Mojsilovic, N. & Stojadinovic, B. A model-order reduction framework for hybrid simulation based on component-mode synthesis. *Earthq. Eng. Struct. Dynam.* **49**, 737–753. https://doi.org/10.1002/eqe.3262 (2020).
38. Maghareh, A. *Nonlinear Robust Framework for Real-Time Hybrid Simulation of Structural Systems : Design , Implementation , and Validation*. Ph.D. thesis, Purdue University (2017).
39. Hammer, T. C., Owen, C. C., van den Berg, M. & Hendrikse, H. Classification of ice-induced vibration regimes of offshore wind turbines. in *Proceedings of the ASME 2022 41st International Conference on Ocean, Offshore and Arctic Engineering*, 1–8. https://doi.org/10.1115/OMAE2022-78972 (OMAE, Hamburg, Germany, 2022).
40. Hammer, T. C., Willems, T. & Hendrikse, H. Dynamic ice loads for offshore wind support structure design. *Mar. Struct.* **87**, 1–19. https://doi.org/10.1016/j.marstruc.2022.103335 (2023).
41. Hammer, T. C. & Hendrikse, H. Experimental study into the effect of wind-ice misalignment on the development of ice-induced vibrations of offshore wind turbines. *Eng. Struct.* **286**, 1–17. https://doi.org/10.1016/j.engstruct.2023.116106 (2023).
42. Hammer, T. C. & Hendrikse, H. On the dependency of the development of frequency lock-in on the mode shape amplitude for higher structural modes. in *Proceedings of the 27th International Conference on Port and Ocean Engineering under Arctic Conditions* (2023).
43. Owen, C. C., Hammer, T. C. & Hendrikse, H. Peak loads during dynamic ice-structure interaction caused by rapid ice strengthening at near-zero relative velocity. *Cold Regions Sci. Technol.* **211**, 103864. https://doi.org/10.1016/j.coldregions.2023.103864 (2023).

Acknowledgements

The authors would like to express their gratitude to the contributing organizations of the SHIVER project: TU Delft, Siemens Gamesa Renewable Energy, and the Dutch Ministry of Economic Affairs and Climate Policy through the 'Toeslag voor Topconsortia voor Kennis en Innovatie (TKI's)' initiative. Special recognition is extended to Otto Puolakka, Teemu Päivärinta and Lasse Turja from the Aalto Ice and Wave Tank, and Arttu

Polojärvi and Alice Petry from Aalto University School of Engineering; Laura van Dijke from TU Delft; Jeffrey Hoek and Tom Willems from Siemens Gamesa Renewable Energy for their help assistance during the test campaign(s). Additionally, credits are given to Marnix van den Berg (former TU Delft), and Kees van Beek and Jeroen Koning (TU Delft) for their help in conceptualizing, manufacturing, programming and troubleshooting the hybrid test setup. During the preparation of this work the authors used ChatGPT 3.5 in order to improve readability of the text passages. After using this tool/service, the authors reviewed and edited the content as needed and take full responsibility for the content of the publication.

Author contributions

Tim. C. Hammer: Conceptualization, Methodology, Software, Validation, Formal analysis, Investigation, Data curation, Writing – original draft, Visualization, Supervision, Project administration **Hayo Hendrikse**: Conceptualization, Methodology, Validation, Investigation, Writing – Review & Editing, Supervision, Project administration, Funding acquisition

Competing interests

The authors declare no competing interests.

Additional information

Correspondence and requests for materials should be addressed to T.C.H.

Reprints and permissions information is available at www.nature.com/reprints.

Publisher's note Springer Nature remains neutral with regard to jurisdictional claims in published maps and institutional affiliations.

Open Access This article is licensed under a Creative Commons Attribution-NonCommercial-NoDerivatives 4.0 International License, which permits any non-commercial use, sharing, distribution and reproduction in any medium or format, as long as you give appropriate credit to the original author(s) and the source, provide a link to the Creative Commons licence, and indicate if you modified the licensed material. You do not have permission under this licence to share adapted material derived from this article or parts of it. The images or other third party material in this article are included in the article's Creative Commons licence, unless indicated otherwise in a credit line to the material. If material is not included in the article's Creative Commons licence and your intended use is not permitted by statutory regulation or exceeds the permitted use, you will need to obtain permission directly from the copyright holder. To view a copy of this licence, visit http://creativecommons.org/licenses/by-nc-nd/4.0/.

© The Author(s) 2024